ELSEVIER

www.elsevier.nl/locate/jelechem

Journal of Electroanalytical Chemistry 497 (2001) 33–46

Journal of Electroanalytical Chemistry

Charge–discharge stability of graphite anodes for lithium-ion batteries

Chunsheng Wang [a,*], A. John Appleby [a], Frank E. Little [b]

[a] *Center for Electrochemical Systems and Hydrogen Research, Texas Engineering Experiment Station, Texas A&M University, College Station, Texas 77843-3402, USA*

[b] *Center for Space Power, Texas Engineering Experiment Station, Texas A&M University, College Station, Texas 77843-3118, USA*

Received 26 May 2000; received in revised form 6 October 2000; accepted 8 October 2000

Abstract

A graphite powder disk sandwiched between two nickel screens was used as a lithium-insertion working electrode. Electrochemical impedance spectroscopy (EIS), galvanostatic intermittent titration (GIT) using pulsed microcurrent, and in-situ intrinsic resistance measurements were used for the evaluation of kinetics and intrinsic (i.e. physical) resistance changes during charge–discharge cycling from room temperature to elevated temperatures. The investigation of the thermal stability of the electrolyte at elevated temperature used an EIS study of a palladium electrode in the electrolyte. EIS measurements for electrochemical reaction and intrinsic resistances of a graphite electrode show that the first high-frequency depressed semicircle is due to the 'solid electrolyte interphase' (SEI) film, although it is also influenced by the electrode contact impedance. The growth of the SEI film on the MCMB 10-28 graphite electrode surface with cycling, results in a decline in kinetic rate and a corresponding increase in contact resistance giving rapid capacity fade. The high stability of the capacity of JM 287 electrodes is due to the slow increase in SEI film thickness on their surfaces. Although new SEI films were formed on the originals at elevated temperature, the kinetics were still more rapid than at room temperature in the initial cycling.

Keywords: Electrochemical reaction kinetics; Intrinsic resistance; Electrochemical impedance spectroscopy; Thermal stability

1. Introduction

Graphite is the most commonly used anode for lithium-ion secondary cells. Good graphite charge–discharge cycle stability is one of the most important criteria for reliable and long-lived lithium-ion battery operation. It is commonly assumed that the composition and structure of the passivation 'solid electrolyte interphase' (SEI) film are both critical for cycling stability. This film results from solvent reduction and decomposition products beginning with the first charge process. The SEI film covering the graphite surface exposed to the electrolyte must be permeable to Li^+ cations, and must be electronically insulating to prevent further electrolyte decomposition during cycling. Further growth will decrease the conductivity of the graphite agglomerate, and reduce the reversible capacity [1–3] due to a decrease in the amount of active material and in the kinetics of lithium insertion. Hence the intrinsic resistance change of a graphite electrode can be used to monitor the formation and growth of SEI film [4,5]. However, how the SEI film directly influences the thermodynamics and electrochemical kinetics of absorption of lithium into graphite is not clear at this time.

Galvanostatic intermittent titration (GIT) is an effective method of measuring the equilibrium potential–composition–temperature isotherm (PCT) during lithium insertion and extraction to and from graphite. The extent of lithium absorption into graphite at a given temperature can be obtained from PCT curves. GIT using pulsed microcurrent can also provide some useful information on the total reaction resistance [5]. One of the more discriminatory methods for measuring electrochemical reaction kinetics is electrochemical impedance spectroscopy (EIS), which can give individual reaction resistances for each step if their time constants are resolvable [6].

* Corresponding author. Fax: +1-409-8459287.
E-mail address: cswang@pop.tamu.edu (C. Wang).

0022-0728/01/$ - see front matter
PII: S0022-0728(00)00447-2

In this work, the cycling stability and kinetics of a lithium–graphite electrode have been studied using in-situ GIT, EIS and in-situ intrinsic resistance measurements. Lithium absorption thermodynamics and kinetics into graphite at 25 and 65°C are compared.

2. Experimental

2.1. Electrode and cell preparation

Two graphite powder samples (MCMB 10-28 and JM 287) were used as anode materials. Their nominal particle size, BET surface area, and source are shown in Table 1.

Composite electrodes were prepared from a mixture of 92 wt% graphite powder with 8 wt% pure polyvinylidene fluoride between two nickel screen current collectors using 1-methyl-2-pyrrolidinone as the solvent. After drying overnight at 120°C, the electrode was pressed into a sandwich structure with a geometric surface area of 2.0 cm^2. The configuration of a typical electrode was shown in a previous paper [5]. The electrodes contained ca. 50 mg of active graphite. Electrochemical measurements were conducted in a special four-electrode PTFE cell. Two lithium foils were used as both counter and reference electrodes, and a Pd wire was used as another working electrode to monitor the stability of the electrolyte at elevated temperature. All potentials given are versus the $Li \mid Li^+$ reference electrode in the experimental electrolyte, which was 1.0 M lithium hexafluorophosphate ($LiPF_6$) in a 1:1 by volume ethylene carbonate (EC) + dimethyl carbonate (DMC) mixture (High Purity Lithium Battery Grade, Mitsubishi Chemical Company). Cells were assembled in an argon-filled glove box. Charge (lithium intercalation) and discharge (lithium extraction) characteristics were measured between +0.0 and +1.5 V at a constant current using an Arbin (College Station, TX) automatic battery cycler.

2.2. In-situ intrinsic resistance measurement

In-situ intrinsic (i.e. physical) resistance of graphite electrodes was carried out using two potentiostats. One was for electrochemical lithium insertion–extraction, and the other was used for measuring intrinsic resistance. A constant current (10 mA for JM 287, and 1 mA for MCMB 10-28 electrodes) was passed across the graphite electrode, and the intrinsic resistance was evaluated from the voltage change between the two sides of the working electrodes. The applied current was chosen so that the voltage between the two sides of the working electrode was less than 10 mV.

To avoid confusion over the various electrode resistances discussed here, the expression intrinsic resistance is used below to refer to those physical elements of resistance which are present within the thickness of the electrode, excluding any electrochemical (faradaic) elements. These include the electronic resistance of the series-parallel array of graphite particles themselves, the transmission line of various contact resistances between the particles including electronic contacts with and within the binder and ionic (electrolytic) contacts, and the electronic resistances of the current collectors and the contact resistances between them and the neighboring graphite particles. This intrinsic resistance may be evaluated by an in-situ direct current method.

2.3. EIS measurement

This was measured over the frequency range 65 kHz to 1.0 mHz at a signal amplitude of 5 mV, using a frequency response analyzer (Solartron, FRA 1250) and an electrochemical interface (Solartron, model 1286). Before EIS measurements, the electrodes were left at open-circuit for 90 min to allow the potential to stabilize. For intrinsic resistance measurement, the EIS was taken: (i) between the two sides of the graphite electrode, connecting terminals RE_2 and WE to one side and RE_1 and CE to the other (called Connection A in the discussion); (ii), as (i), with RE_2 and WE to one side and CE to the other, with a lithium foil connected to RE_1 as a reference electrode (Connection B). For electrochemical reaction kinetics measurements, three EIS scans were made using different methods of connecting the Solatron 1286 electrochemical interface terminal to the graphite electrode. In the first scan, terminals RE_2 plus WE were connected to both sides of the graphite electrode (Connection C); in the second scan, terminals RE_2 plus WE were connected to one side only (Connection D); and in the third scan, terminal RE_2 was connected to one side and terminal WE to the other (Connection E). The differences between the three EIS scans thus obtained allow determination of the influence of contact resistance on the electrochemical reaction kinetics.

Table 1
Nominal particle sizes and BET surface areas of graphite powders

Sample	Nominal particle size/um	BET surface area/$m^2\ g^{-1}$	Distributor
MCMB 10-28	10	1.5	Osaka Chemical Co.
JM 287	<15	13.5	Johnson Matthey

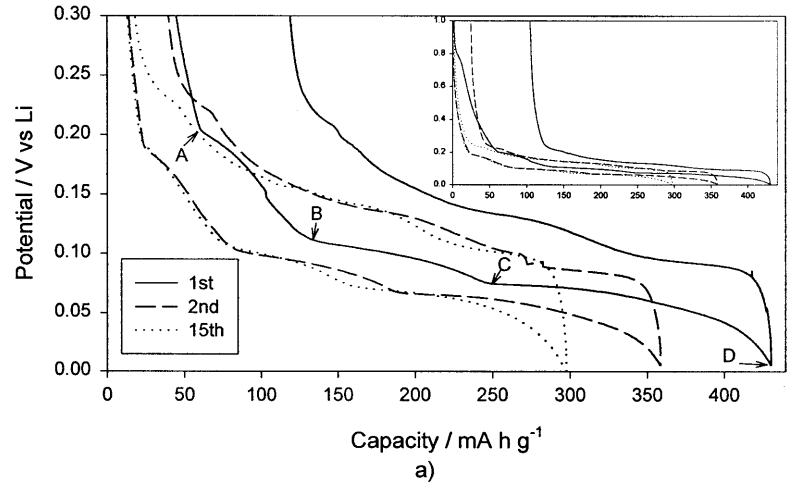

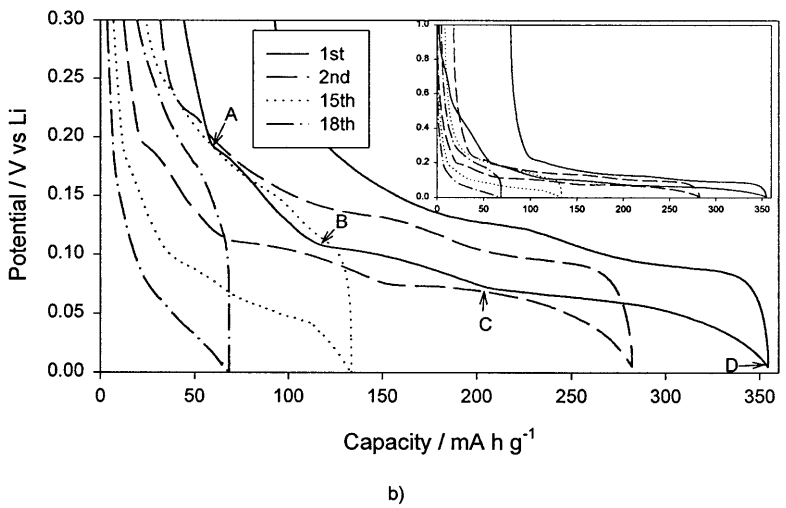

Fig. 1. Potential profiles of graphite electrodes during charge–discharge cycles 1, 2, and 15. A–B, B–C, and C–D correspond to the lithium capacity of the three phase zones. (a) JM 287; cycling current, 5.1 mA g^{-1}; (b) MCMB 10-28; cycling current, 3.4 mA g^{-1}. The insets in the right corner show the expanded potential range.

2.4. GIT measurement

Lithium was inserted or extracted to or from the graphite electrode in a series of current pulses of equal duration (1.0 h), such that the overall time required to pass 372 mA h g^{-1} of capacity was 72 h (C/72 rate). Following each current pulse, the cell was allowed to relax for 2.5 h. The potential was logged at regular time intervals by computerized data acquisition. Simultaneously, a 10 mA (or 1 mA for MCMB 10-28 graphite) dc current was passed through the graphite electrode to obtain the intrinsic resistance. A low charge–discharge current of 0.25 mA (5.1 mA g^{-1}) was used to ensure a low overpotential (< 10 mV) and the long charge–discharge time (1.0 h) ensured the system was in a pseudo-steady state. The long open-circuit relaxation time was used to ensure an equilibrium open-circuit potential. Hence, the lithium insertion–extraction reaction resistance at different lithium contents could be calculated directly from the ratio of overpotential to charge–discharge current, and the intrinsic resistance of graphite could be obtained without interference from this current. In GIT measurement, the relaxation time interval between successive insertion (or extraction) steps is rather critical, since it should be long enough to ensure the establishment of equilibrium, yet short enough to prevent loss of lithium by self-discharge. All reaction and intrinsic resistances, whether measured from EIS or GIT, were normalized to the weight of the graphite electrode.

Table 2
Capacity data for JM and MCMB 1028 graphite

	JM graphite			
	Charge capacity mAh g^{-1} Q_c	Discharge capacity mAh g^{-1} Q_d	Irreversible capacity mAh g^{-1} Q_{irr}	Relative irreversible capacity [a]/%
1st	430	332	98	22.8
2nd	360	338	22	61
15th	295	295	0	
	MCMB graphite			
	Charge capacity mAh g^{-1} Q_c	Discharge capacity mAh g^{-1} Q_d	Irreversible capacity mAh g^{-1} Q_{irr}	Relative irreversible capacity [a]/%
1st	355	280	75	21.1
2nd	282	266	16	60.1
15th	133	126	7	

[a] Relative irreversible capacity = Q_{irr}/Q_c.

3. Results and discussion

3.1. Charge–discharge stability of graphite anodes at 25°C

3.1.1. Capacity–Potential Profiles

Fig. 1 shows the potential profiles of JM 287 and MCMB 10-28 graphites in Cycles 1, 2, and 15, and Table 2 summarizes their capacities. For clarity, the lithium insertion capacity is subdivided into three phase transformation zones (A–B, B–C, C–D). Rate of capacity fade on cycling in the three phase transformation zones is shown in Table 3. The results may be summarized as follows:

1. The Irreversible capacity above 0.2 V for both graphites is similar, although the total irreversible capacity of JM 287 is larger than that of MCMB 10-28.
2. The reversible capacity decay of JM 287 is less than that of MCMB 10-28, whose gradual increase in charge–discharge potential hysteresis on cycling indicates slowing of the reaction kinetics.
3. Capacity fade in the three zones is similar, so the decrease in total active graphite because of disintegration or electrolyte insertion must affect the capacity decline.

Since the kinetics fade of MCMB 10-28 is faster than that of JM 287, its capacity change as a function of rate should also be less. Fig. 2 shows that its capacity rapidly decreased with increasing cycling current, characterized by larger potential hysteresis.

3.1.2. GIT and in-situ intrinsic electrode resistance measurements

Fig. 3 shows the open-circuit potential and intrinsic resistance profiles at Cycles 9 and 16 for the two graphites under GIT conditions. While the lithium absorption capability decreased 8.3% for JM 287 and 35% for MCMB 10-28, the open circuit potentials in the three phase zones are similar, indicating a stable graphite structure on cycling. The capacity decline may be attributed to the loss of active graphite and an increase in overpotential, which decreases the time to 0.0 V. Reaction resistance peaks were observed at the ends of the three potential plateaus, which indicate higher lithium diffusion resistance [5]. The average reaction resistances and peak heights increased with cycling, especially for MCMB 10-28, which in contrast to JM 287 also showed a large increase in intrinsic resistance.

To summarize, capacity fade on cycling is characterized by increases in intrinsic and reaction resistances, presumably induced by the continued growth of the SEI film. This growth increases the current collector-powder and powder–powder contact resistance, as measured by the in situ dc method [5] and the SEI film and charge transfer resistances measured by GIT. For further resistance separation, EIS may be used.

3.1.3. EIS measurement

This was used to investigate the reaction resistance and intrinsic resistance for both graphites on Cycles 10 and 17. For measurement of electrochemical reaction kinetics, the signal was applied to both sides of the

Table 3
Rate of capacity fade of JM 287 and MCMB 1028 graphite in three phase transformation zones

	MCMB 1028			JM 287		
Cycle number	A–B	B–C	C–D	A–B	B–C	C–D
1st	1.0	1.0	1.0	1.0	1.0	1.0
2nd	0.86	0.89	0.92	0.86	0.88	0.94
15th	0.43	0.40	0.43	0.71	0.75	0.75

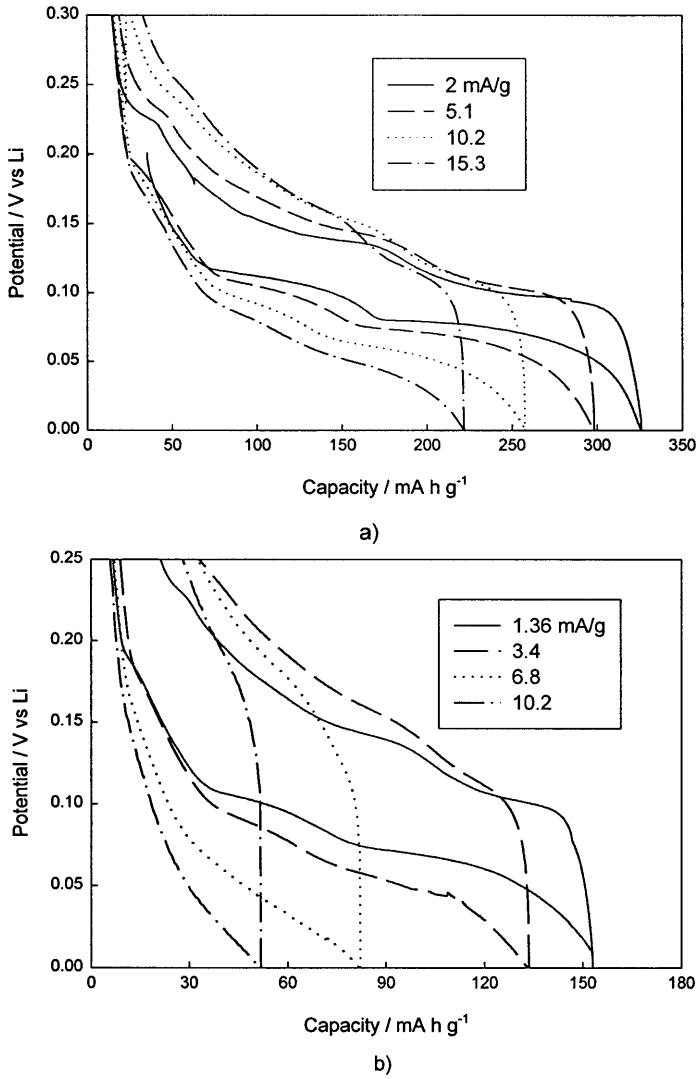

Fig. 2. Potential profiles as a function of cycle current after 9 previous cycles. (a) JM 287; (b) MCMB 10-28.

graphite working electrode (Connection C), and for intrinsic resistance, the EIS was determined between the two sides of the graphite electrode (Connection A). Fig. 4 shows impedance spectra for the electrochemical reaction and electrode impedance of MCMB 10-28 at different lithium contents on the above cycles. All the reaction spectra (Fig. 4(a)) have similar features: two medium-to-high frequency depressed semicircles, and an inclined low frequency line. It is generally considered that the two semicircles are for the SEI and interfacial charge transfer impedances, respectively, while the inclined line is the lithium diffusion impedance [5,7]. Recently Chang and Sohn have proposed that the first depressed high-frequency semicircle is for contact resistance between electrode particles and the current collector [8]. The present experiments show that it is associated with the SEI film, but graphite particle-to-current collector and particle-to-particle resistances must also be involved, because the SEI is present everywhere (see Section 3.1.4). The two depressed semicircles in the intrinsic resistance spectra (Fig. 4(b)) are indeed for graphite particle-to-current collector and particle-to-particle resistance [5]. Fig. 4(a) shows an large increase in diameter of the first (high-frequency) semicircle from Cycle 10 to 17, showing that the resistance of the SEI film on MCMB 10-28 graphite grows rapidly in this cycle range. This resistance increase is attributed to the SEI film growth because the capacitances, which are inversely proportional to the film thickness, rapidly decrease in this cycle range. Therefore the large increase in GIT reaction resistance (Fig. 3(b)) must involve continued SEI growth, which increases the particle contact resistances (Fig. 4(b)).

In contrast, only small corresponding resistance increases were observed for JM 287 graphite (Fig. 5(a)), and the intrinsic resistance was stable between Cycles 10 and 17 (Fig. 5(b)). In the latter, the resistance determined from the intersection of the high-frequency line with the real axis is the graphite electronic resis-

tance and the small semicircle is for the particle-to-current collector contact impedance [5]. The high-frequency reactance in the EIS for intrinsic resistance is an instrumental artifact which disappears when the measured resistance is high [5]. The results in Fig. 5(b) suggest that SEI growth on JM 287 graphite is only from graphite particles to the bulk electrolyte, and not between particles.

3.1.4. EIS characterization

As stated in the Section 2, three different kinetic EIS studies and two intrinsic resistance studies each using a different connection protocol were used. These allow certain distinctions to be made. For example, if the first high-frequency depressed semicircle in the kinetic resistance EIS is for graphite particle-to-current collector contact resistance, as Chang and Sohn [8] suggest, the diameter of the first semicircle using Connection D should be twice that determined for that using Connection C (see Fig. 6) since the graphite particle-current collector area is thereby doubled. In addition, this first semicircle should not be present in EIS measurements using Connection E (see Fig. 6) because this protocol automatically eliminates the intrinsic resistance of the graphite electrode. The intrinsic resistance EIS using Connection B (Fig. 6) should similarly reflect the influence of the intrinsic graphite electrode impedance on that for lithium kinetics.

Fig. 7(a, b) shows the results of the three protocols for JM 287 kinetic impedance measurements and the two for its intrinsic impedance after 17 cycles at 25°C followed by 3 cycles at 65°C. The purpose of cycling JM 287 at 65°C is to increase the SEI film thickness [9], which will be reflected in the Nyquist plot of EIS. Fig. 7 shows that at the same lithium content, the diameter of the first depressed semicircle increases when the temperature is decreased from 65 to 25°C, with a further small decrease on charging with lithium under these conditions (Fig. 7(a)). The real resistance of the first semicircle at 63 mV and 25°C (Fig. 7(a)) is larger

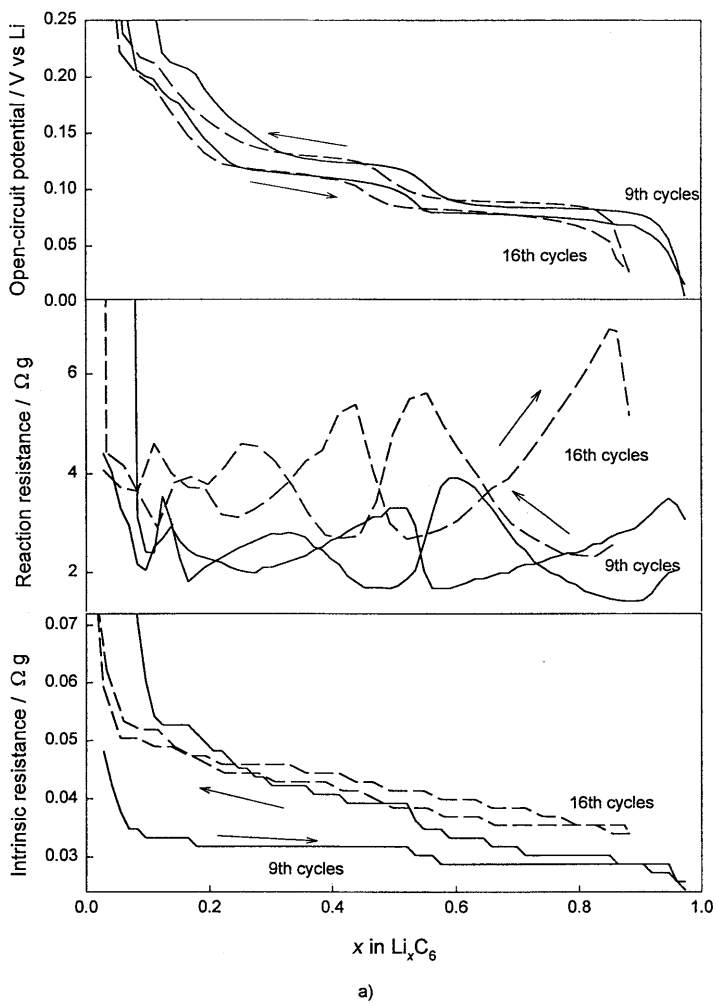

Fig. 3. Dependence of open-circuit potential, intrinsic resistance and reaction resistance on cycles 9 and 16. Charge–discharge current: 5.1 mA g^{-1}. Galvanostatic current pulses are on for 1.0 h, off for 2.5 h. (a) JM 287; (b) MCMB 10-28.

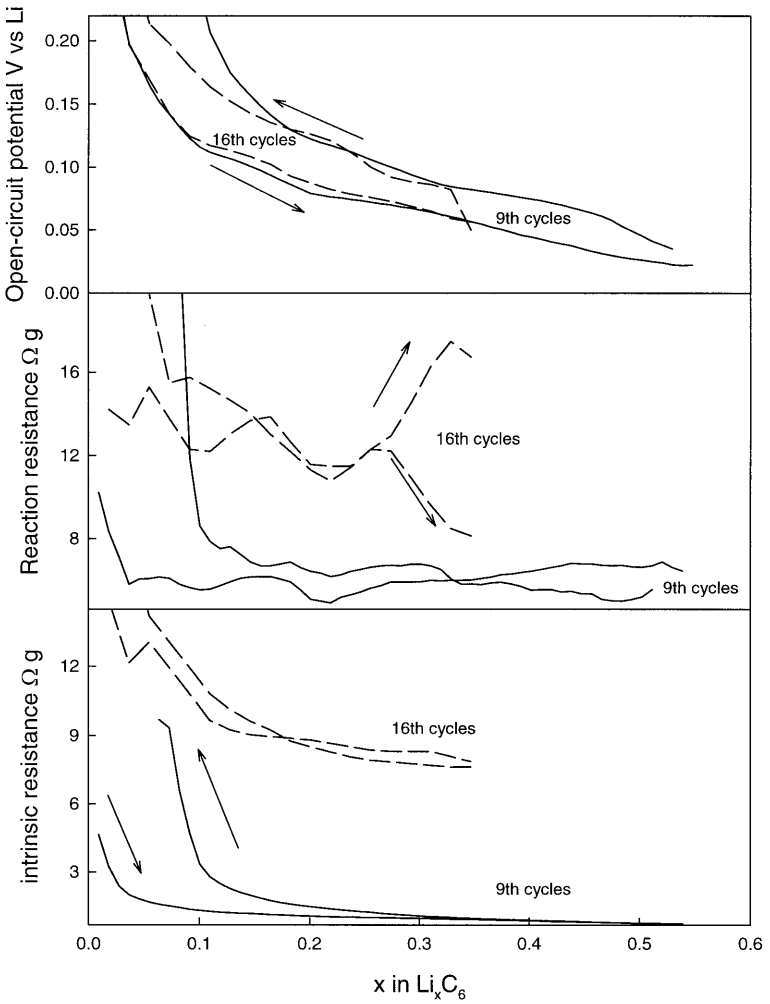

b)

Fig. 3. (*Continued*)

than that before cycling at 65°C (Fig. 5(a)), which suggested that the first depressed semicircle is related to SEI film.

Fig. 7 also shows that the first depressed semicircle is present in the EIS using Connection E, and is smaller than that using Connection D (see Fig. 6). The first semicircle in the Connection C plots (Fig. 6) lies midway between those in the Connection E and D plots, and is less than half the size of that using Connection D, as would be expected from Ref. [8]. The contact resistance for the Connection E plot is zero, whereas that for the Connection C plot should be half of that for Connection D. Hence, the first semicircle in the Connection C plot should indeed lie between those in the plots for Connections E and D. The results in Fig. 7(a) strongly suggest that the first high-frequency depressed semicircle in the Connection C or D plots is mainly related to the SEI film resistance, but the intrinsic resistance of the graphite electrode increases its diameter somewhat.

The intrinsic impedance data in Fig. 7(b) show that both measurements of the intrinsic impedance (Connections A and B) consist of three semicircles at 65°C, which become two at 25°C. These result from the particle-to-particle and particle-to-current collector contact resistances [5]. The impedance from Connection B has a similar shape to that corresponding to Connection A, but the former is almost half the size of the latter. Thus the overall increase in resistance resulting from the intrinsic electrode resistance is only about half of the real intrinsic graphite electrode resistance.

Using these conclusions, the graphite electrode equivalent circuit of Funabiki et al. [7] should be modified as shown in Fig. 6. It consists of four parallel resistance–capacitance (R/C) circuits in series, the first two being for the graphite particles-to-current collector and particles-to-particles contact impedances, respectively. R_G, R_{RG}, and R_{CG} are the electronic graphite resistance, reference electrode-to-anode electrolyte resistance, and reference electrode-to-counter electrode electrolyte re-

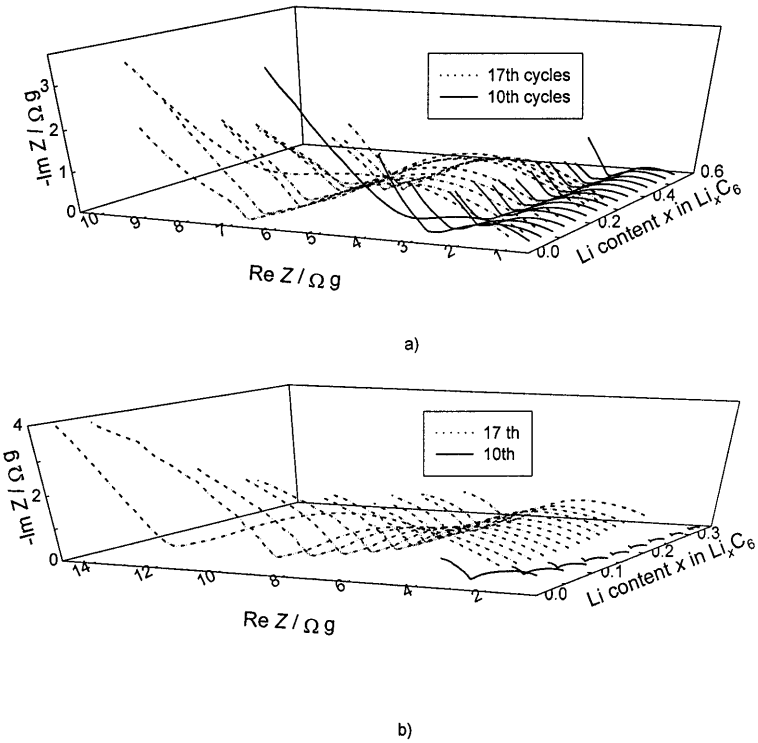

Fig. 4. Nyquist plots demonstrating: (a) kinetics of lithium insertion–extraction; (b) intrinsic impedance of MCMB 10-28 graphite as a function of lithium content on cycles 10 and 17.

sistance. R_{pc}, R_{pp}, R_{SEI} and R_{ct} are the graphite particles-to-current collector, particles-to-particles, SEI film, and charge–transfer resistances. C_{pc} and C_{pp} are the particles-to-current collector and particles-to-particles contact capacitances. Q_{SEI} and Q_{dl} are constant-phase elements for the SEI film and the double-layer, respectively, Z_w is the semi-infinite lithium diffusion Warburg impedance, and C_Φ is a pseudocapacitance. Here R_{SEI}/Q_{SEI} can be considered as two or three R/C circuits in series due to the SEI film of a multilayer structure, c.f. the similar equivalent circuit given by Levi and Aurbach [10]. However, these authors relate each of the four R/C circuits to Li^+ migration through one SEI film layers, whereas here the two R/Cs are attributed to particle-to-collector and particle-to-particles contact impedances.

The fitted curve in Fig. 7(a) (at 60°C and 0.93 V) shows that simulation based on equivalent circuits in Fig. 6 results in a good fit to the experimental data. However excellent agreement between simulation and experiment cannot be used to confirm a real equivalent circuit, because such complex impedance spectra may be reproduced by a number of different equivalent circuits [10]. Further experiments were therefore conducted to verify certain aspects of the equivalent circuit in Fig. 6.

Fig. 6 shows that the EIS using Connection E will become the same as that for Connection D if the Solatron electrochemical interface terminal WE is moved from one side of the graphite electrode (G_2) to the other (G_1). If terminal CE is moved from the lithium foil counter electrode to the G_2 side of the electrode, the EIS using Connection D will become the same as that for Connection B. The EIS using Connection E will then reflect the impedance of electrochemical lithium insertion into graphite with no influence from the intrinsic electrode resistance.

The EIS using Connection B is the intrinsic resistance of the graphite electrode during kinetic EIS measurements, and that using Connection D is the total impedance for lithium insertion. If the intrinsic impedance is in series with that for lithium insertion, the impedance using Connection D should be equal to the sum of the impedances using Connections E and B, i.e.

$$Z_D = Z_E + Z_B$$

Fig. 7(a) show that the sums of Z_E and Z_B (the line) in three cases are exactly the same as Z_D (points), confirming the equivalent circuit in Fig. 6. It is interesting that the intrinsic graphite electrode impedance measured via Connection B is equal to 45% of the real intrinsic impedance (measured via Connection A) at high potential and about 40% of it at low potential (see the line and points on the left of Fig. 7(b)). Further, the characteristic frequency of Z_B is the same as that of Z_A, indicating that both refer to the same reaction. Why Z_B should be about 50% of Z_A may be explained as follows.

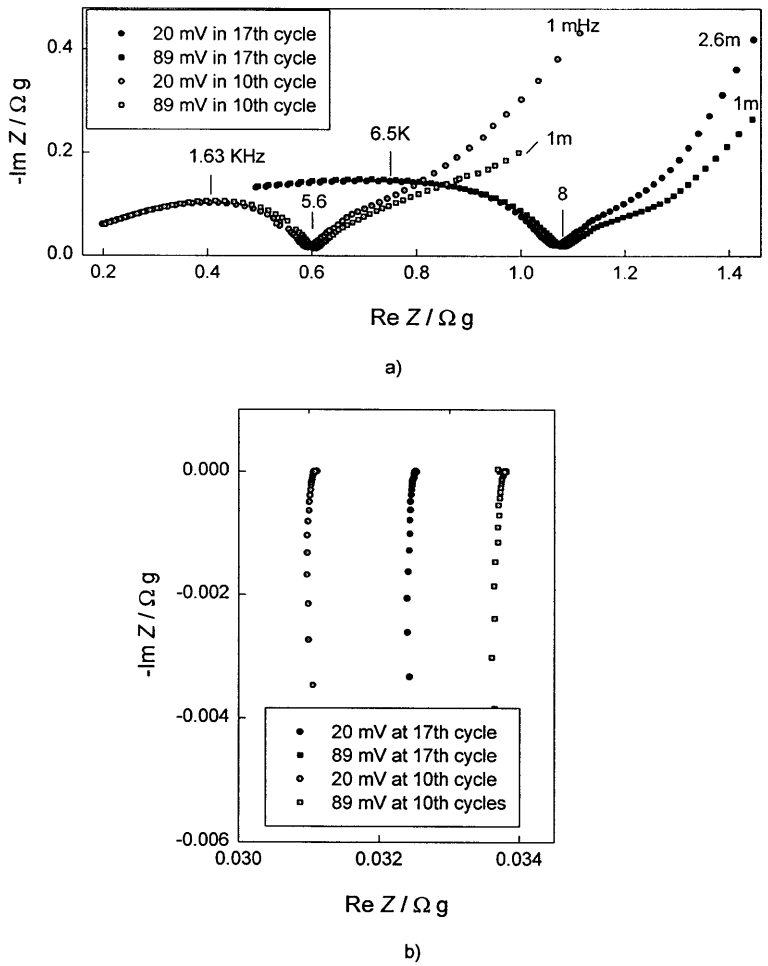

Fig. 5. Nyquist plots demonstrating: (a) kinetics of lithium insertion–extraction; (b) intrinsic impedance of JM 287 graphite at potentials of 20 and 89 mV, cycles 10 and 17.

If the RE_1 terminal is moved from G_2 to the lithium reference electrode under Connection A conditions, the circuit will become equivalent to Connection B. Under the latter conditions, a ± 5 mV (to Li reference) sinusoidal voltage signal applied to one side of the graphite electrode results in a total signal of ± 10 mV across both sides, so that the impedance measured using Connection B will be apparently half of that using Connection A.

In the measurement of intrinsic impedance measurements, a sinusoidal voltage signal applied between the two sides of the electrode will result in a similar lithium charge current on one side and lithium discharge on the other. The electrochemical reaction impedance is generally higher than the intrinsic impedance, so the influence of parallel electrochemical impedance is small.

3.2. Stability of graphite anodes at 65°C

3.2.1. EIS on graphite electrodes at 65°C

Accelerating rate calorimeter (ARC) results have led to the conclusion that the SEI film initially formed at ordinary temperatures is metastable, and converts slowly to a stable phase [11,12]. It is believed that the final film is less passivating than the metastable phase, since it permits continued film growth [9,13]. Fig. 8 shows the rate of lithium self-discharge on open circuit (via the change in open-circuit potential as a function of time) from fully-charged JM 287 at 25°C (thick solid line) and at 65°C. The self-discharge rate of JM graphite at 65°C is much higher than that at 25°C.

The conversion of SEI film from a metastable to a stable phase, and its subsequent growth at high temperature will change the resistance of the film. This can be monitored by EIS because the first depressed high-frequency semicircle is dominated by SEI film properties if the intrinsic electrode resistance is not too large (see Section 3.1.4). The reaction and intrinsic EIS plots in Figs. 9 and 10 were obtained at points A–N in Fig. 8. In this work, the fully charged JM 287 graphite electrode was first left on open-circuit at 25°C for 800 h, then was again fully charged, left at 65°C for 35 h, then again left at 25°C for 32 h. The purpose of resting at 25°C after 35 h at 65°C is to eliminate the influence of

the higher temperature on the EIS. After 3 charge–discharge cycles at 65°C the fully charged JM 287 graphite was held at 65°C for 230 h. The first 35 h period at 65°C was to allow investigation of the conversion of the SEI film from a metastable to a stable phase. The second 230 h period at 65°C was to monitor SEI film growth at high temperature.

Fig. 9(a) shows that only a small increase in SEI resistance (i.e. little change in potential) was observed over 800 h on open circuit at 25°C. This results from a small amount of SEI growth, since a small decrease in Q_{SEI} occurred during this open circuit period, as is shown by fitting the parameters to the equivalent circuit in Fig. 6. However, the EIS at 65°C (at point C) shows a very small initial semicircle, which shows a small decrease in diameter over the next 35 h. The low resistance of the first semicircle results from the high conductivity of both the SEI and the electrolyte at 65°C. The subsequent decrease in resistance of the first semicircle may result from conversion of the SEI film from a metastable to a stable phase. To avoid the influence of changing temperature on the conductivity of both SEI and electrolyte, the cell was cooled to 25°C after 35 h on open-circuit at 65°C. The EIS taken at point F (25°C, at 39 h) shows that the real resistance for the first semicircle (0.73 Ω g) is smaller than that at points A, G, and B (1.07, 0.89, and 1.8 Ω g, at 3, 65, and 800 h at open-circuit at 25°C). However, it is much larger than that at point E (35 h at 65°C, 0.33 Ω g). If the SEI film observed over 35 h at 65°C is the stable phase (as we suppose), then this film has a lower resistance than the metastable phase. The increase in resistance at point G over a further 26 h at 25°C must result from newly formed metastable film. The continued growth of stable SEI film was observed during the 230 h period at 65°C (dotted lines in Figs. 8 and 10(a)). The conversion of the SEI film from a metastable to a stable phase at 65°C had little influence on the intrinsic resistance of JM 287 graphite (Fig. 9(b)). However, growth of the stable SEI film on the JM 287 graphite surface rapidly increased the intrinsic resistance of the electrode (Fig. 10(b)). The above conclusions on the change of the SEI film with time are in general agreement with ARC [11,12] and capacity variation [9] results.

3.2.2. Electrolyte stability at 65°C

To determine the resistance of the SEI film accurately, it is necessary to know whether the electrolyte is stable, because the electrolyte conductivity is in series with the electrochemical reaction impedance as shown in Fig. 6. Therefore, a change in electrolyte conductivity due to thermal or electrochemical reaction of the electrolyte will affect the total resistance in the high

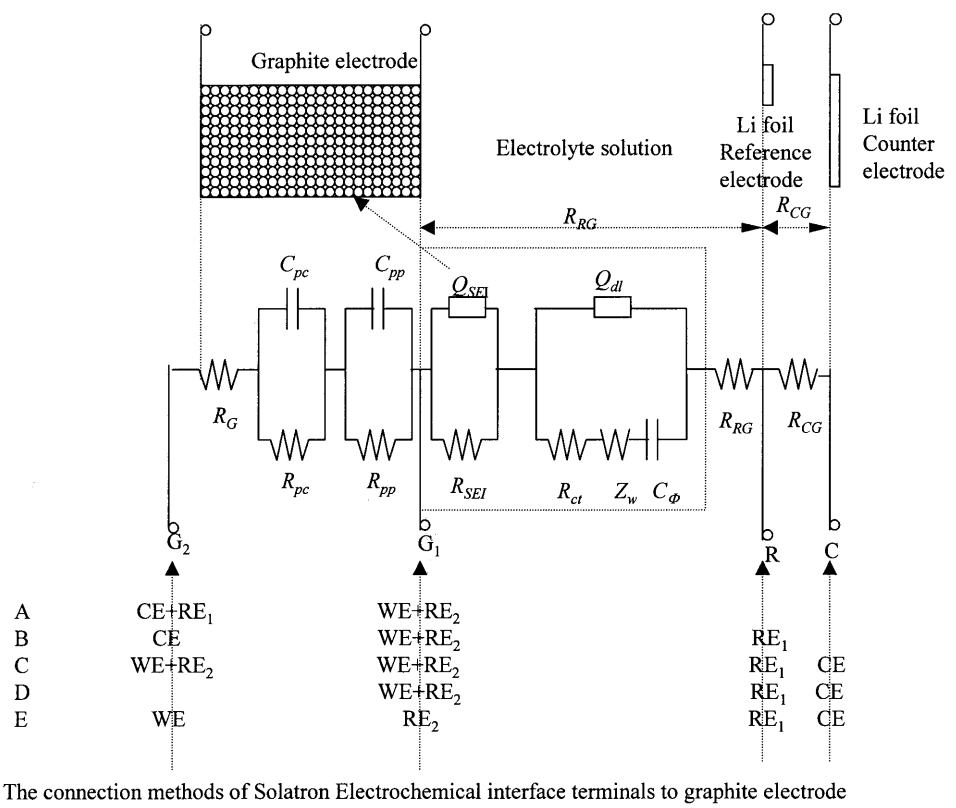

Fig. 6. Equivalent circuit of graphite electrodes (modified from Funabiki Ref. [7]). A schematic diagram of the cell and different Solatron electrochemical interface terminal-to-electrode connections (Fig. 7) is also shown.

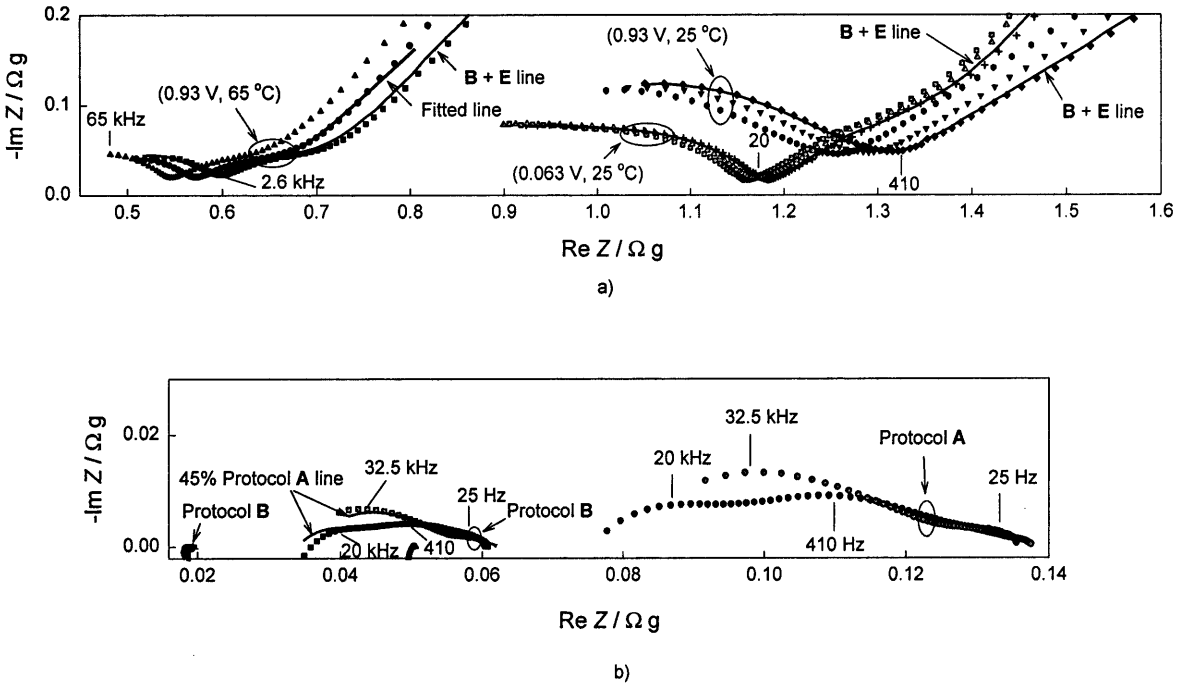

Fig. 7. Nyquist plots demonstrating: impedance of JM 287 graphite using different Solatron electrochemical interface terminal-to-electrode connections. (a) reaction kinetic impedance of lithium insertion–extraction; ● Protocol C (0.93 V, 65°C); ■ Protocol D (0.93 V, 65°C); ▲ Protocol E (0.93 V, 65°C); ▼ Protocol C (0.93 V, 25°C); ◆ Protocol D (0.93 V, 25°C); ★ Protocol E (0.93 V, 25°C); ► Protocol D (0.063 V, 25°C); □ Protocol E (0.063 V, 25°C); △ Protocol C (0.063 V, 25°C). (b) intrinsic impedance, ● Protocol A (0.93 V, 65°C); ■ Protocol B (0.93 V, 65°C); ○ Protocol A (0.93 V, 25°C); □ Protocol B (0.93 V, 25°C); ▲ Protocol A (0.063 V, 25°C); ▼ Protocol B (0.063 V, 25°C). Before measurement, the electrode was cycled 17 times at 25°C, then 3 times at 65°C.

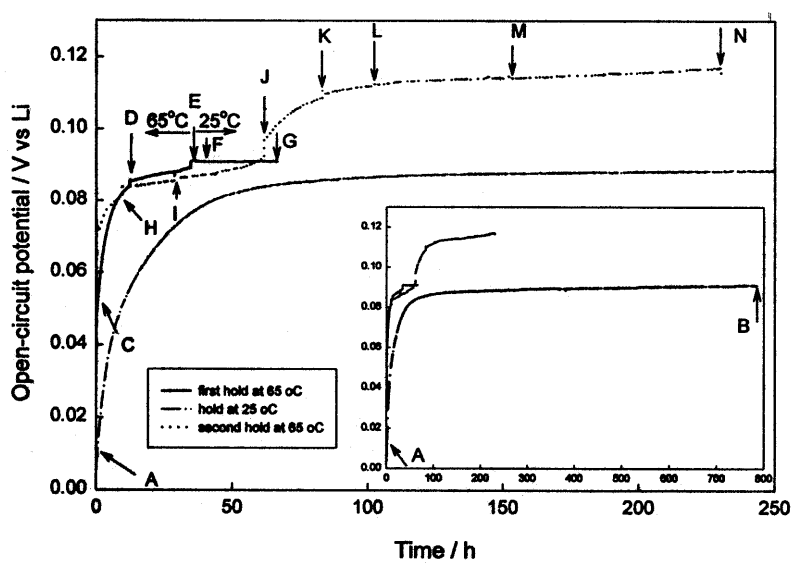

Fig. 8. Potential profiles of JM 287 electrode on open circuit at 25 and 65°C as a function of time. The fully charged JM 287 graphite electrode was first left on open-circuit at 25°C for 800 h (point A–B), then was again fully charged, left at 65°C for 35 h, then again left at 25°C for 32 h (point C–G). After 3 charge–discharge cycles at 65°C the fully charged JM 287 graphite was held at 65°C for 230 h (point H–N). EIS results were obtained at A–N.

frequency region. The thermal stability of the electrolyte used in this work was examined via EIS data on stable palladium wire electrodes as a function of time at open circuit (i.e. uncharged with lithium) at 25 and 65°C. Fig. 11 shows Nyquist plots of a floating Pd electrode in the high frequency range. The intersection of the high-frequency lines with the real axis indicate electrolyte resistance. The cell was not calibrated, and

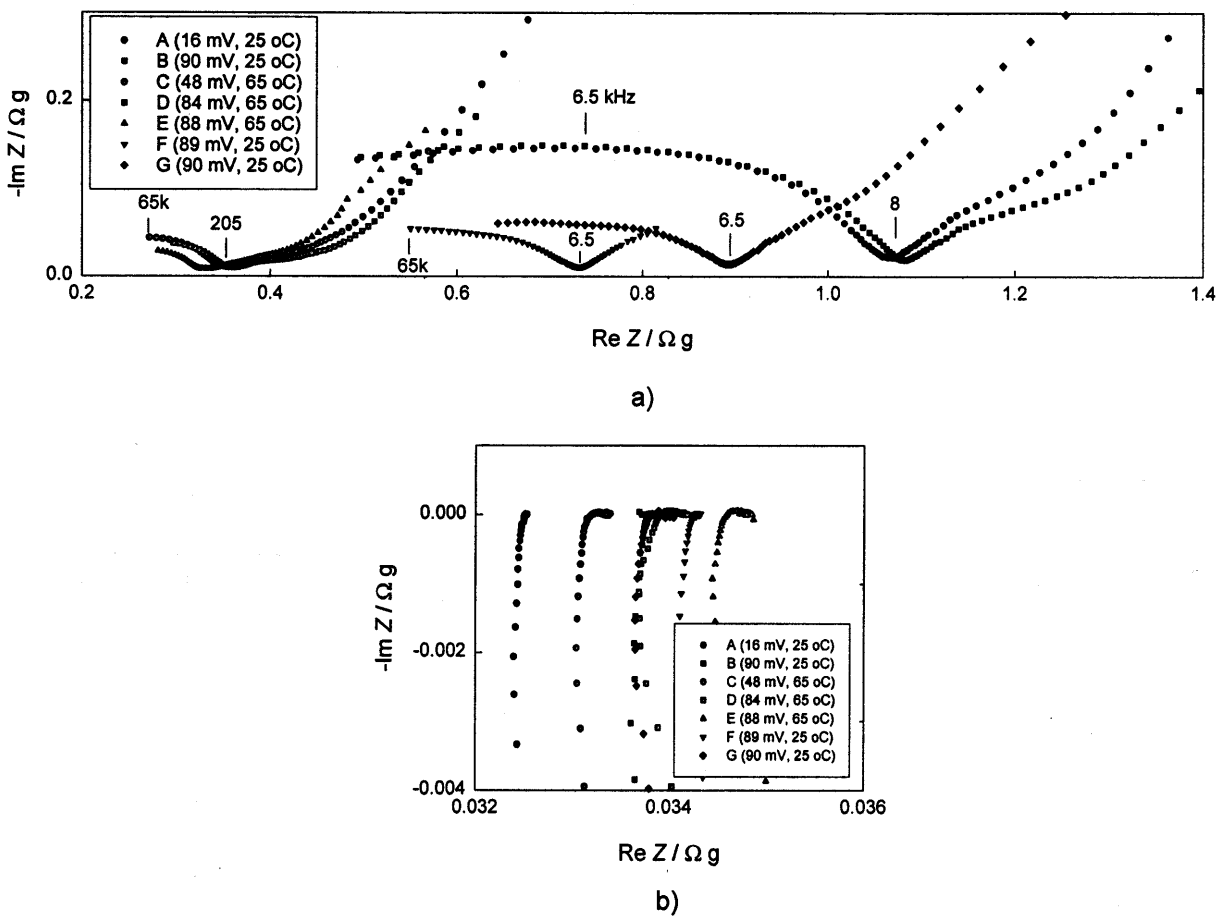

Fig. 9. Nyquist plots for JM 287 electrode at 25 and 65°C (points A–G, Fig. 8). (a) For lithium insertion–extraction kinetics measured using C protocol; (b) Intrinsic resistance measured using A protocol.

the relative changes show that the increase in conductivity with temperature is high, but only a 7% reduction in conductivity occurred after 15 days at 65°C, which indicates that the electrolyte is relatively stable at this temperature.

3.2.3. GIT and in-situ intrinsic resistance at 65°C

After the 65 and 25°C EIS measurements, the JM 287 electrode was cycled at 65°C using the same C/72 current pulses as at room temperature. After two complete cycles, GIT and in-situ intrinsic electrode resistance results were obtained. Fig. 12 shows the open-circuit potential, reaction resistance, and intrinsic resistance graphite under these conditions. For comparison, results on cycle 17 at room temperature are included.

It is evident that temperature has little effect on open-circuit potential, but a large irreversible capacity was observed because of SEI film growth. As expected, the average electrochemical reaction resistance is lower at 65°C than that in room temperature, so the kinetics will be improved under equal SEI film conditions.

4. Conclusions

The effects of temperature on the electrochemical characteristics of lithium-insertion secondary anodes have been investigated using GIT, EIS, and in-situ intrinsic resistance measurement on JM 287 and MCMB 10-28 graphite in 1.0 M lithium hexafluorophosphate in 1:1 by volume ethylene carbonate + dimethyl carbonate. EIS of a floating palladium wire electrode was used to verify electrolyte stability under electrochemically neutral conditions. Progressive SEI film growth on graphite increased both the electrochemical reaction resistance and the particle-to-current collector and particle-to-particles contact resistance, which result in capacity fade on cycling. The electrolyte itself is stable at 65°C under non-reducing conductions. This investigation provides direct EIS evidence for the slow decomposition of the metastable SEI film formed at room temperature to a more stable product. In addition, fresh layers can grow on top of metastable films, which confirms earlier studies using ARC [11,12] and capacity variation [9]. Contrary to other results [8],

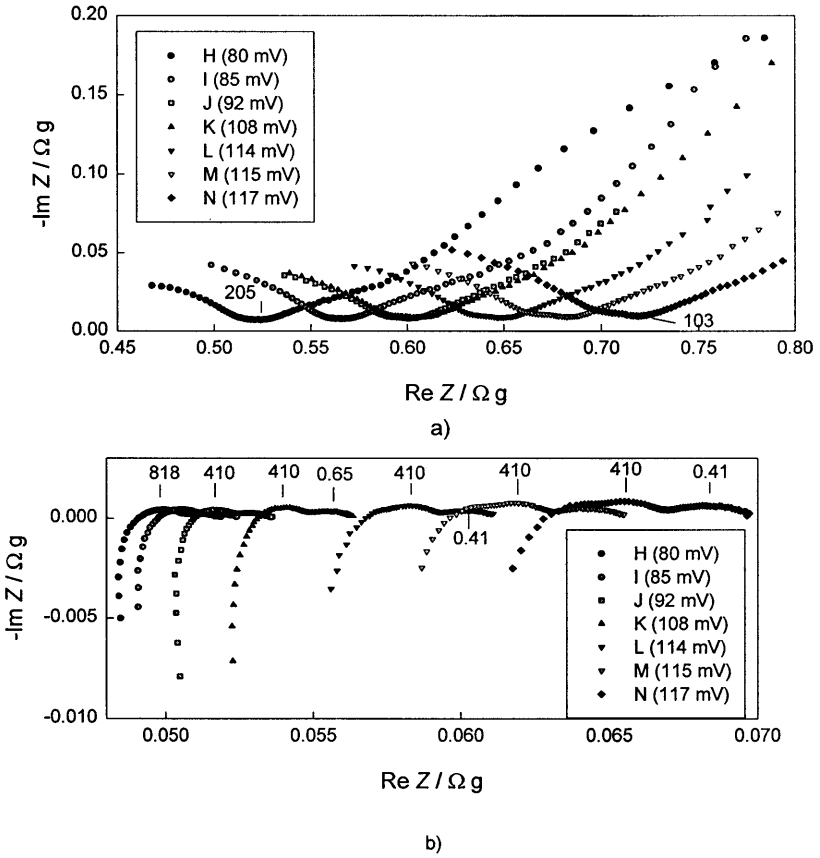

Fig. 10. Nyquist plots for JM 287 electrode at 65°C (point H–N, Fig. 8). (a) For lithium insertion–extraction kinetics measured using C protocol; (b) Intrinsic resistance measured using A protocol.

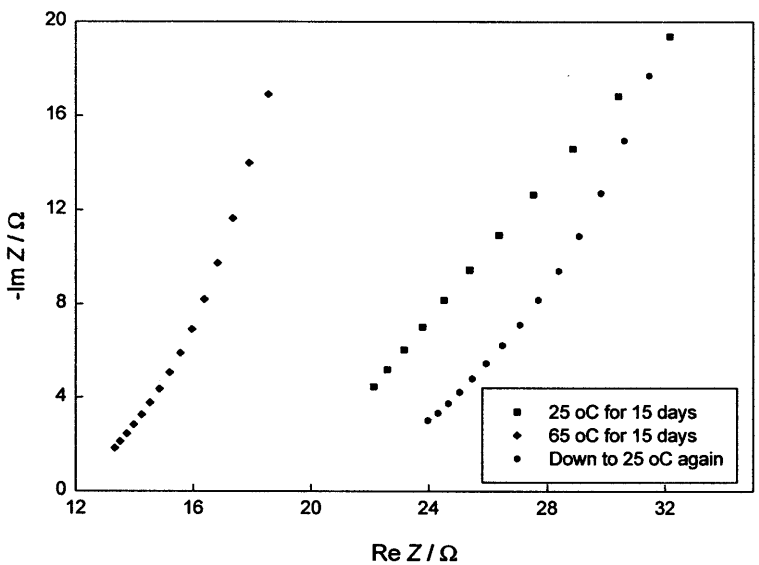

Fig. 11. High frequency spectra Nyquist plots for palladium wire electrode in the experimental electrolyte at 25 and 65°C.

EIS of graphite anodes shows that the first depressed semicircle may be attributed to the presence of the SEI film, with some influence from the intrinsic electrode resistance.

Acknowledgements

We gratefully acknowledge NASA-Glenn Research Center, Cleveland OH, for support of this work.

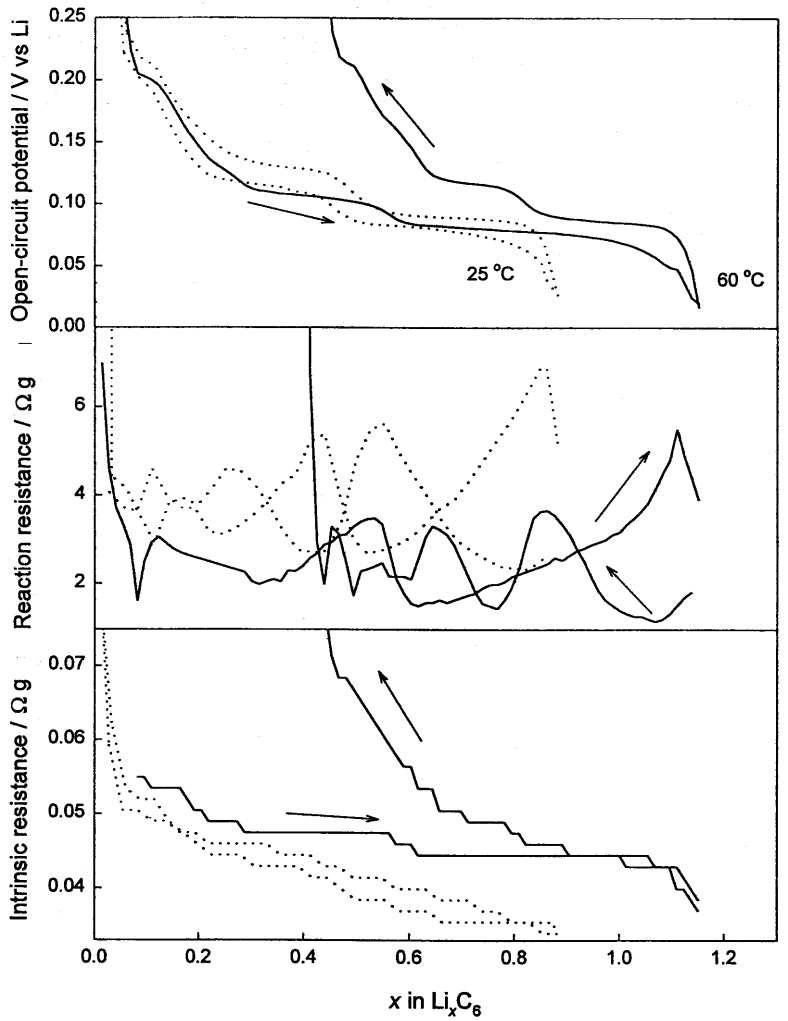

Fig. 12. Open-circuit potential, intrinsic resistance and reaction resistance for JM 287 electrode at 25 and 65°C. 25°C data measured after 17 cycles, 65°C data after 3 cycles, both at the experimental temperature. Charge–discharge current: 5.1 mA g^{-1}. Galvanostatic current pulses were on for 1.0 h, off for 2.5 h.

References

[1] T. Takamura, H. Awano, T. Ura, K. Sumiya, J. Power Sources 68 (1997) 114.
[2] M. Saito, A. Shimokawa, K. Sekine, T. Takamura, Ext. Abst. 196th Electrochem. Soc. Mtg., Honolulu HI, The Electrochemical Society, Pennington NJ, 1999, Abst. No. 242.
[3] D. Aurbach, B. Markovsky, A. Nimberger, Electrochim. Acta 45 (1999) 67.
[4] M. Nishizawa, H. Koshika, I. Uchida, J. Phys. Chem. B103 (1999) 192.
[5] C.S. Wang, I. Kakwan, A.J. Appleby, F.E. Little, J. Electroanal. Chem. 489 (2000) 55.
[6] C.S. Wang, J. Electrochem. Soc. 145 (1801) 1998.
[7] A. Funabiki, M. Inaba, Z. Ogumi, S.I. Yuasa, J. Ostuji, A. Tasaka, J. Electrochem. Soc. 145 (1998) 172.
[8] Y.C. Chang, H.J. Sohn, J. Electrochem. Soc. 147 (2000) 50.
[9] T. Zhang, A.S. Gozdz, G. Amatucci, J. Electrochem. Soc. 146 (1999) 4014.
[10] M.D. Levi, D. Aurbach, J. Phys. Chem. B101 (1997) 4630.
[11] M.N. Richard, J.R. Dahn, J. Electrochem. Soc. 146 (1999) 2068.
[12] D.D. MacNeil, D. Larcher, J.R. Dahn, J. Electrochem. Soc. 146 (1999) 3596.
[13] A.M. Andersson, K. Edstrom, N. Rao, A. Wendsjo, J. Power Sources 81–82 (1999) 268.